Available online at www.sciencedirect.com

ScienceDirect

journal homepage: www.elsevier.com/locate/he

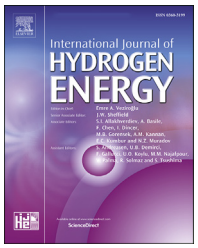

Experimental and kinetic study of laminar flame characteristics of H_2/O_2/diluent flame under elevated pressure

Xin Lu [a,b], *Erjiang Hu* [a,*], *Sage Kokjohn* [b], *Qunfei Gao* [a], *Geyuan Yin* [a], *Ke Zeng* [a], *Zuohua Huang* [a,**]

[a] *State Key Laboratory of Multiphase Flow in Power Engineering, Xi'an Jiaotong University, Xi'an, People's Republic of China*

[b] *Engine Research Center, University of Wisconsin-Madison, Madison, United States*

HIGHLIGHTS

- Laminar burning velocity and flame instability of diluted H_2 flame were studied.
- The effects of pressure, diluent and equivalence ratios were studied.
- A non-monotonic pressure dependence of laminar burning velocity was observed.
- A new correlation allowing for this non-monotonic behavior was presented.

ARTICLE INFO

Article history:
Received 28 May 2020
Received in revised form
15 August 2020
Accepted 17 August 2020
Available online 19 September 2020

Keywords:
Laminar burning velocity
Flame instability
Markstein length
Hydrogen flame
Diluents
Elevated pressure

ABSTRACT

Laminar burning velocity, Markstein length, and critical flame radius of an H_2/O_2 flame with different diluents, He, Ar, N_2 and CO_2, were measured under elevated pressure with different diluent concentrations. The effects of pressures, diluents, and dilution and equivalence ratios were studied by comparing calculated and experimental results. The laminar burning velocity showed non-monotonic behavior with pressure when the dilution ratio was low. The reason is the radical pool reduced with increasing pressure and leads to the decrease of overall reaction order from larger than 2 to smaller than 2, and further leads to this non-monotonic phenomenon. A modified empirical equation was presented to capture the relationship between active radicals and laminar burning velocity. Critical radii and Markstein lengths both decrease with initial pressure and increase with equivalence ratio and dilution ratio. The calculated critical radii indicate that the Peclet number and flame thickness control the change of R_{cr}. It can be found that Le_{eff} has a significant influence on Peclet number and leads to the decrease of critical flame radii of Ar, N_2, and CO_2 diluted mixture. Interestingly, the CO_2 diluted mixture has the lowest Markstein length under stoichiometric conditions and a high value under fuel-rich conditions, consistent as the flame instability observed on the flame images. The reason is that the Le_{eff} of CO_2 diluted mixture increased rapidly with the equivalence ratio.

* *Corresponding author*. State Key Laboratory of Multiphase Flow in Power Engineering, Xi'an Jiaotong University, Xi'an, 710049, People's Republic of China.
** *Corresponding author*. State Key Laboratory of Multiphase Flow in Power Engineering, Xi'an Jiaotong University, Xi'an, 710049, People's Republic of China.
E-mail addresses: hujiang@mail.xjtu.edu.cn (E. Hu), zhhuang@mail.xjtu.edu.cn (Z. Huang).
https://doi.org/10.1016/j.ijhydene.2020.08.142

Introduction

Hydrogen has been gaining scholarly attention recently due to its potential application in the future transportation industry. It provides power for vehicles by both internal combustion engines [1–3] and fuel cells [4–6]. Besides, the oxidation of hydrogen is important as an essential subset mechanism of oxidation of any hydrocarbon fuel [7]. Studying the hydrogen flame with different diluents also contributes to the oxidation mechanism of hydrocarbon under similar conditions. The effects of diluents on hydrogen flames were studied both experimentally and computationally in this work.

Laminar burning velocity provides validation information for chemical mechanisms [8]. Additionally, it is relevant to the turbulent burning velocity and contributes to the design of combustion devices. However, for hydrogen flames under high pressure and fuel-lean conditions, flame instability can be enhanced, which can lead to the self-acceleration of the flame propagation speed [9–11]. This can result in faster propagation speed, which is not captured by the chemical mechanism predictions. Thus, research on both laminar burning velocity and flame instability can provide essential information about hydrogen combustion.

There has been a flourishing discussion on the idea of using diluents. Qiao et al. [12] studied the effects of diluents on H_2/air flame with the dilution of He, Ar, N_2, and CO_2 under atmospheric and sub-atmospheric pressure and further expanded the experiments under microgravity and reduced pressure [13]. A number of studies has looked at H_2/air [14,15], syngas/air [16,17], and hydrocarbon/H_2/air [18,19] with extra N_2 and CO_2 to simulate the Exhaust gas recirculation (EGR) conditions. Additionally, Helium is widely adopted in researching high-pressure laminar flames [20–23] because its high diffusivity helps to smooth the flame front. To better understanding the chemical effects on H_2 laminar burning velocity, some researchers reported empirical fittings [12,24,25] that the relationship between laminar burning velocity and active radicals. Looking beyond this frequently discussed relationship under atmospheric or sub-atmospheric pressured conditions, validations of high-pressure experiments are still scarce. The majority of previous researches [12–15] focused on the effects of diluents on hydrogen/air flames. Thus, the separated effects of diluents on H_2 flames become complicated with these mixtures because there always exists N_2. Therefore, the mixtures in this work consist of H_2, O_2, and one single diluent. Additionally, the pressure dependence of hydrogen with different diluents has received little attention. The non-monotonic behavior of the laminar burning velocity with pressure was reported in He diluted flames [20]; yet whether this behavior also exists with other diluents remains to be clarified. Therefore, a study of H_2/O_2/diluent flames under elevated pressures is warranted to rule out the effects of diluents on hydrogen flame.

This study aims to examine the effects of diluents, pressure, equivalence ratios, and diluent concentrations on laminar burning velocity and flame instability. The Markstein length and critical flame radius are measured to study flame instability. The effects of physical factors on flame instability are studied experimentally and theoretically. The laminar burning velocity is measured and compared with the calculated results using a detailed chemical reaction mechanism, which is also used for further chemical analysis. A new empirical equation is presented to predict the relationship between laminar burning velocity and active radicals under elevated pressure.

Experimental and simulation methods

Experimental apparatus

The experiments were performed in a constant volume combustion chamber [26,27] with a length of 210 mm and an inner diameter of 180 mm, as shown in Fig. 1. During the experiments, the initial temperature and pressure were controlled by the temperature and pressure monitoring system. The combustion chamber was filled with the premixed mixture in advance. The mixture was then ignited by a spark generated by a pair of centrally placed electrodes. Flame images were recorded by a high-speed camera, which works at a speed of 20,000 frames per second. The images were used for the extraction of laminar burning velocities and Markstein lengths.

The premixed mixture was prepared in a 20-L mixing tank using the partial method, as recommended by Xiouris et al. [28]. Experiments of the same equivalence ratio use the same mixture to reduce the random error in equivalence ratio. To prepare the mixture, the tank was first evacuated to vacuum, and the components were filled into the tanks by the order of H_2, O_2, and diluents (N_2/CO_2/He/Ar). The tank was then allowed to sit for at least 8 h to ensure uniform distribution. The uncertainty of the pressure transducer is ±0.02 kPa, while the pressure of the premixed mixture in the mixing tank was 0.8 MPa. The purity of all gases was above 99.5%.

The experimental conditions are listed in Table 1. Four different diluents, N_2, He, Ar, and CO_2, were used in the experiments. The concentration of oxygen is defined as the dilution ratio, which is defined as the volume of diluents normalized by the volume of oxygen: $D = V_{diluent}/V_{O2}$. For example, the dilution ratio of air is 3.762. In this work, three different dilution ratios were studied. Those are $D = 4$, 7, and 10, which represent that the O_2 concentrations are 20% O_2/80% diluent, 12.5% O_2/87.5% diluent and 9.1% O_2/90.9% diluent, respectively. For He, Ar and N_2 diluted mixtures, dilution ratios of 4, 7, and 10 are used. For the CO_2 diluted mixture, only a dilution ratio of 4 was studied because the mixture could not be ignited at other dilution ratios.

The laminar burning velocity and Markstein length can only be measured when the flame surface is smooth. When the diluted mixture is under lean and high-pressure conditions, a cellular structure appeared and the author measured the critical radius of flame instability, which is defined as the onset [29–31] of flame self-acceleration.

Extrapolation of laminar burning velocity

The local flame radius, R_f, was extracted from the original images using a circle-fitting algorithm. Flame radii between 9 and 25 mm were used for accurate extrapolation of laminar

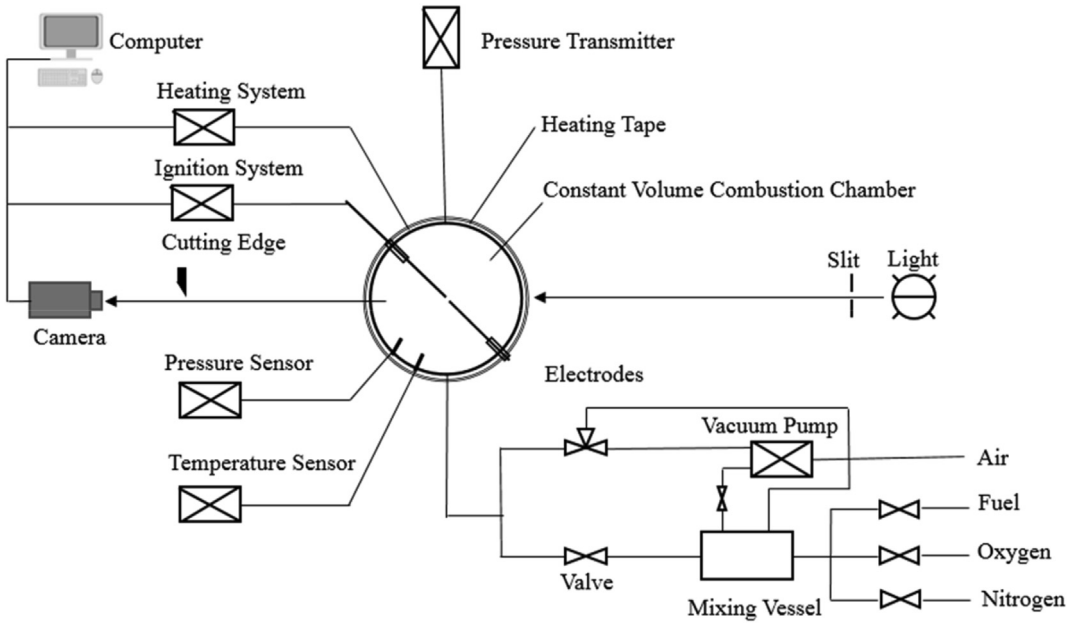

Fig. 1 – Diagram of the experimental apparatus.

Table 1 – Experimental conditions.

Mixture	Diluent Ratio	Equivalence ratio	Temperature (K)	Pressure (MPa)
$H_2/O_2/N_2$	4, 7, 10	0.7, 1.0, 3.0	298	0.1, 0.2, 0.4
$H_2/O_2/He$	4, 7, 10	0.7, 1.0, 3.0	298	0.1, 0.2, 0.4
$H_2/O_2/Ar$	4, 7, 10	0.7, 1.0, 3.0	298	0.1, 0.2, 0.4
$H_2/O_2/CO_2$	4	0.7, 1.0, 3.0	298	0.1, 0.2, 0.4

burning velocity and Markstein length. 9 mm was used to avoid the effects of ignition energy, and 25 mm was used for the upper limit to avoid the effects of the cylinder wall, according to 30% of cylinder radius [32].

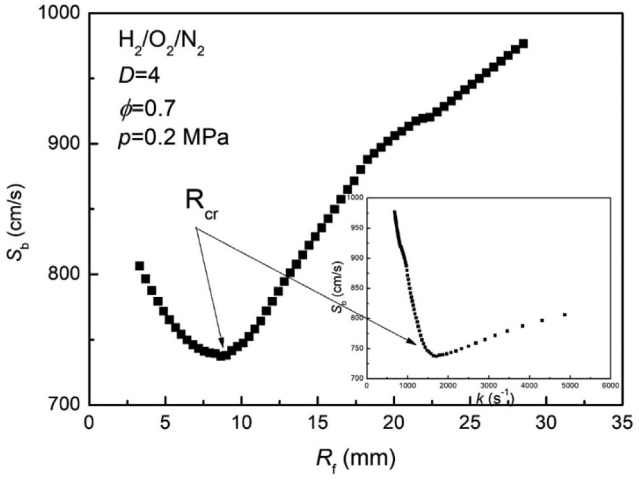

Fig. 2 – The definition of the critical flame radius.

The raw flame radius as a function of time was smoothed using a Savitzky – Golay filter [33]. The flame propagation speed, S_b, was obtained from the derivative of the flame radius concerning the time

$$S_n = \frac{dr_f}{dt} \tag{1}$$

where t is the time after ignition. The unstretched flame propagation speed, S_b^0, was extrapolated using the non-linear method [33,34] by

$$\frac{S_b}{S_b^0} = 1 - \frac{2L_b}{R_f}, \tag{2}$$

where L_b is the Markstein length. The laminar burning velocity, S_u, was obtained from mass conservation of the burned and unburned mixture given by

$$S_u \cdot \rho_u = S_b \cdot \rho_b = f_0, \tag{3}$$

where ρ_u and ρ_b are the density of the unburned and burned mixture, and f_0 is the mass burning rate.

The critical flame radius

At some experimental conditions, a cellular structure appears and experimental L_b is unavailable. For conditions where

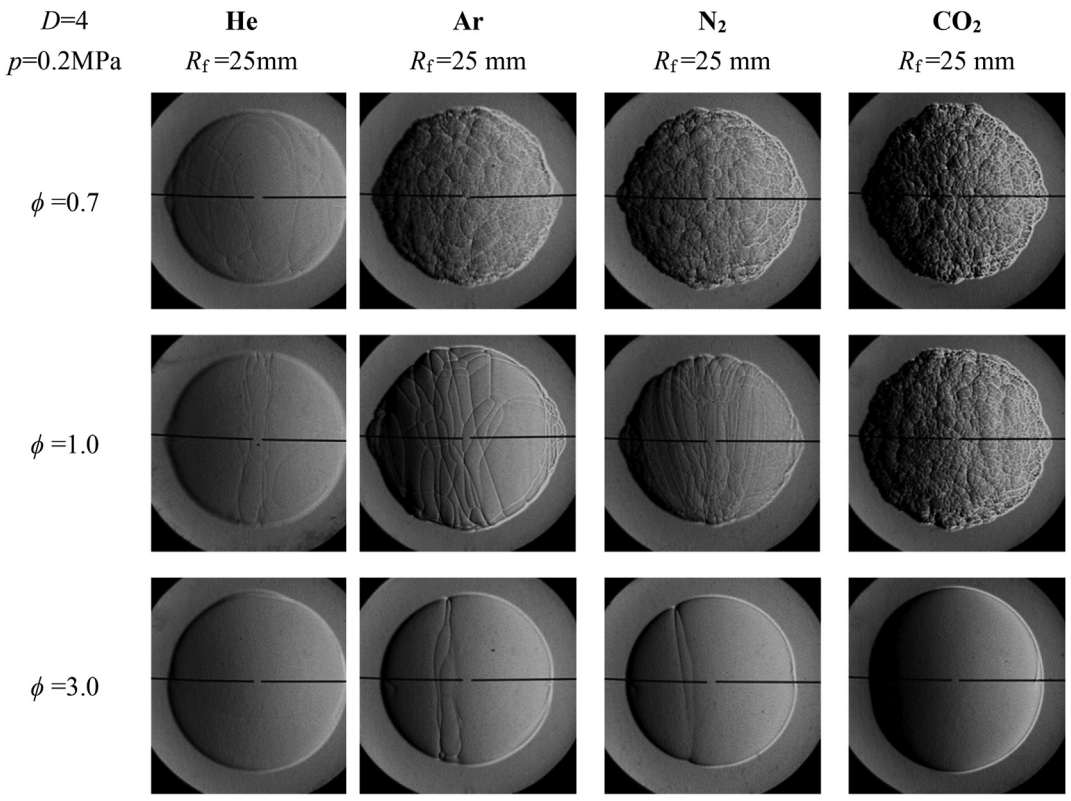

(a)

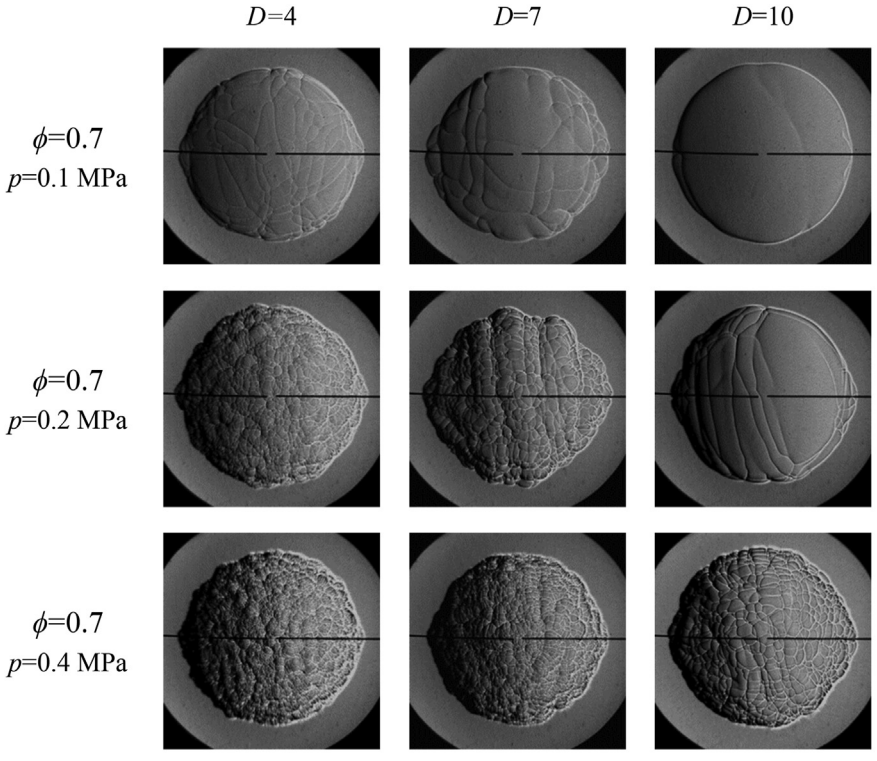

(b)

Fig. 3 – (a) Flame images of different diluents and equivalence ratios and (b) flame images of Ar diluted mixtures of different dilution ratios and pressures.

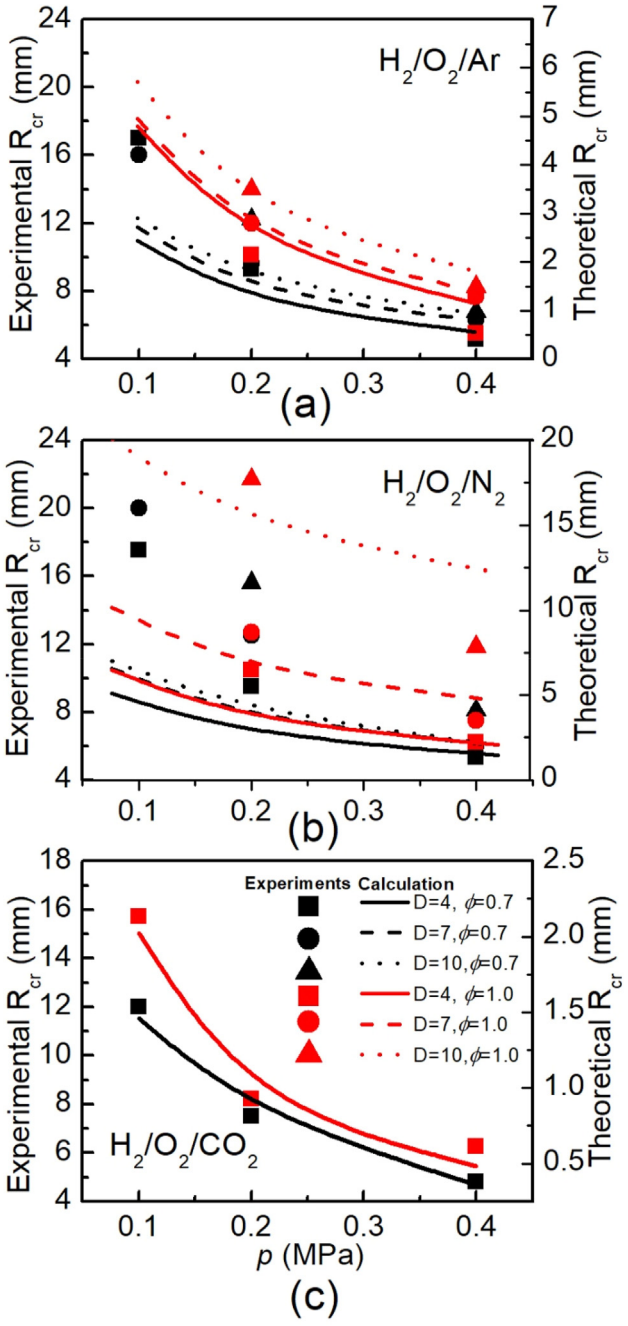

Fig. 4 – Critical radii of different mixtures as a function of pressure.

flame instability appears at R_f larger than 15 mm, there is still enough data (R_f = 9–15 mm, more than 30 points of data) to extract S_u and L_b; thus, both the critical flame radius and Markstein length at these conditions are presented. The critical flame radius is introduced to study flame instability. Fig. 2 shows the definition of the critical flame radius. It can be seen that the flame propagation speed initially decreases with increasing flame radius, then rapidly increases because of the unstable flame front. Thus, the onset of this self-acceleration is defined as the critical radius, R_{cr}. The critical Peclet number, $Pe_{cr} = R_{cr}/\delta$, is a non-dimensional number that represents flame instability. To study the effects of physical factors, the theoretical Pe_{cr} was calculated with Addabbo's theory [34].

$$\frac{1}{A}\frac{dA}{dt} = \frac{\dot{R}_f}{R_f}\left(\omega - \frac{\delta}{R_f}\Omega\right). \tag{4}$$

At the critical radius, the growth rate is zero and the critical Peclet number can be expressed as

$$Pe_{cr} = \frac{\Omega}{\omega}, \tag{5}$$

where the coefficients ω and Ω are given by

$$\omega = \left[-(b-a) + \sqrt{(b-a)^2 - 4ac}\right] \Big/ 2a, \tag{6}$$

$$\Omega = \omega^{-1}\left\{Q_1 + \left[Ze(Le_{eff} - 1)/(\sigma - 1)\right]Q_2 + PrQ_3\right\}, \tag{7}$$

where the coefficients a, b, c, Q_1, Q_2, and Q_3 are given in Addabbo's work [34], and Pr is the Prandtl number. l_0, Ze, and Le_{eff} are the flame thickness, Zel'dovich number, and the effective Lewis number. The flame thickness is given by

$$l_0 = \frac{\lambda}{\rho_u S_u^0 Cp}, \tag{8}$$

where λ and C_p are the thermal conductivity and the heat capacity of the unburned mixture. The Zel'dovich number [35] is

$$Ze = \frac{Ea(T_{ad} - T_u)}{R\,T_{ad}^2}, \tag{9}$$

where T_u and T_{ad} are the unburned temperature and adiabatic flame temperature, respectively. R is the ideal gas constant, which is 8.314 J/(mol·K). Ea is the overall activation energy, as given in [35].

$$Ea = -\frac{2R \cdot \partial \ln(S_u \cdot \rho_u)}{\partial(1/T_{ad})}. \tag{10}$$

The Lewis number represents the thermal and mass diffusivities and is given by

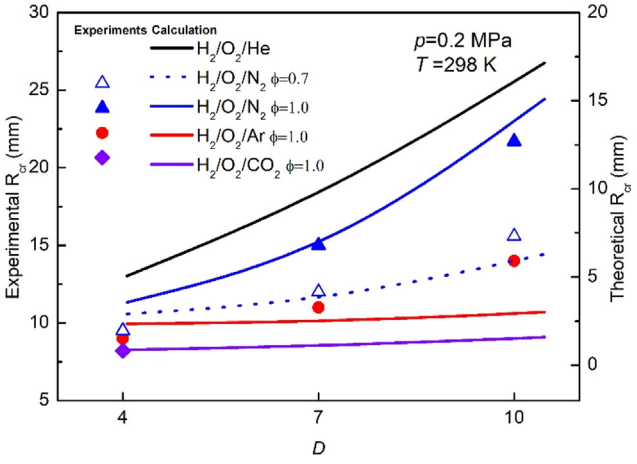

Fig. 5 – Comparison of the critical radius of mixtures with different diluents as functions of the dilution ratio.

$$Le = \frac{\lambda}{\rho_u C_p D}, \tag{11}$$

where D is the binary diffusion coefficient of deficient reactants and the diluents. At the stoichiometric ratio, there is no deficient reactants since all the reaction are consumed. However, Le near the stoichiometric ratio is meaningless according to the definition. Thus, the effective Lewis number, Le_{eff}, was used to study the diffusivity. According to Bechtold et al. [36], the effective Lewis number was given by

$$Le_{eff} = 1 + \frac{Le_E - 1 + (Le_D - 1)\mathscr{A}}{1 + \mathscr{A}}, \tag{12}$$

where $\mathscr{A} = 1 + Ze(\Phi - 1)$, and Φ is the ratio of mass of excess-to-deficient reactants. Le_D and Le_E are the Lewis numbers of excess and deficient reactants.

Experimental uncertainty

The diluted mixtures were studied under lean, rich, and stoichiometric conditions, with an initial temperature of 298 K and initial pressures from 0.1–0.4 MPa. The uncertainty of initial temperature is ±2K, while that of initial pressure is ±0.01 kPa. Both systematic and random uncertainties were considered for laminar burning velocity and Markstein length. The experimental uncertainty was evaluated with the method proposed by Moffat [37]. The effects of equivalence ratio, dilution ratio, pressure, and radiation [38] were considered for the systematic uncertainty. The total uncertainty of the laminar burning velocity is 0.5%–5%. The total uncertainty of the Markstein length is 2%–10%. Uncertainty in the critical flame radius only considers random uncertainty, which is 10–20%. The details of uncertainty analysis are available in previous research [20,39].

Numerical methods

In this study, a detailed chemical model modified by Burke [40] was used for chemical calculation. This mechanism was well validated by experiments under various conditions. The laminar burning velocity was calculated using Chemkin II [41] and the Premix code [42]. The radical mole fractions were also obtained using the Premix code. Soret diffusion effects and

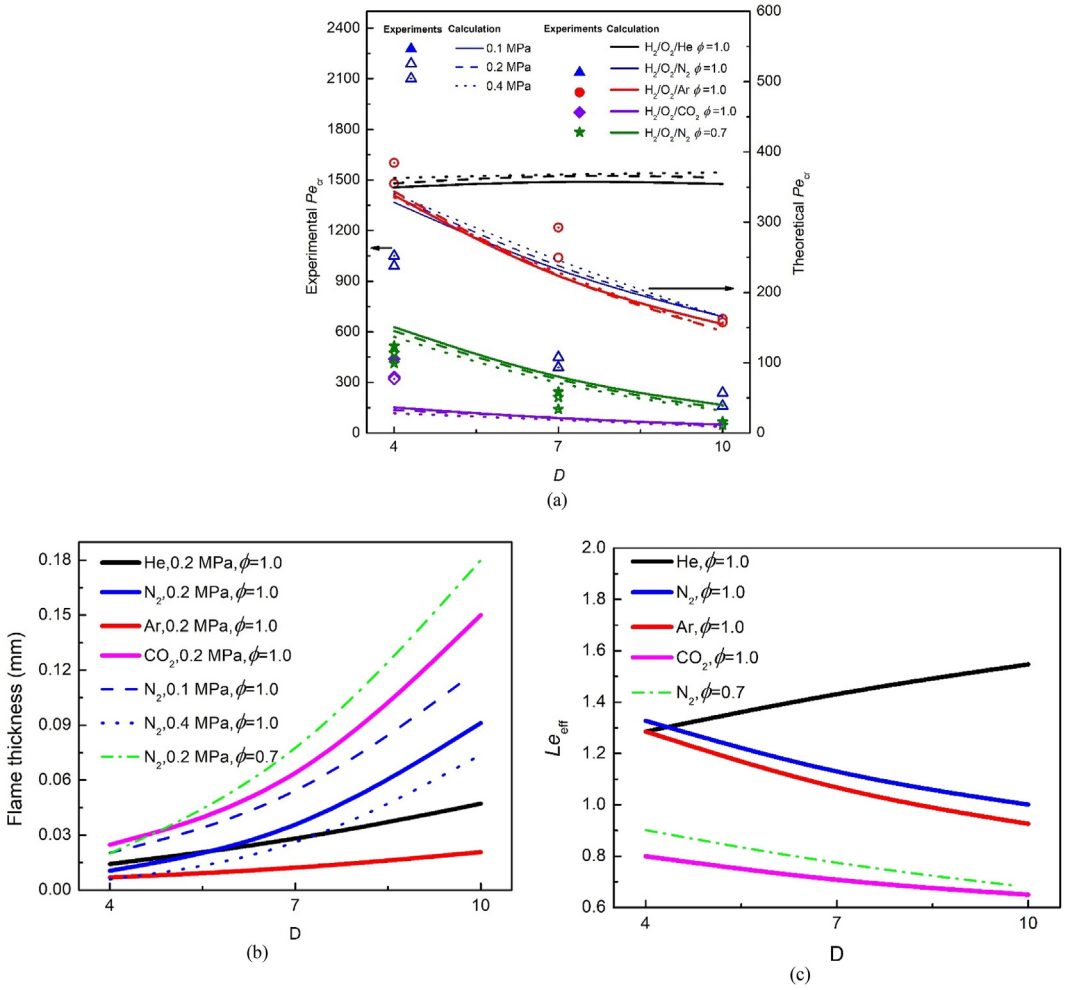

Fig. 6 – (a) Critical Peclet Number, (b) flame thickness, and (c) effective Lewis number of different mixtures at different conditions.

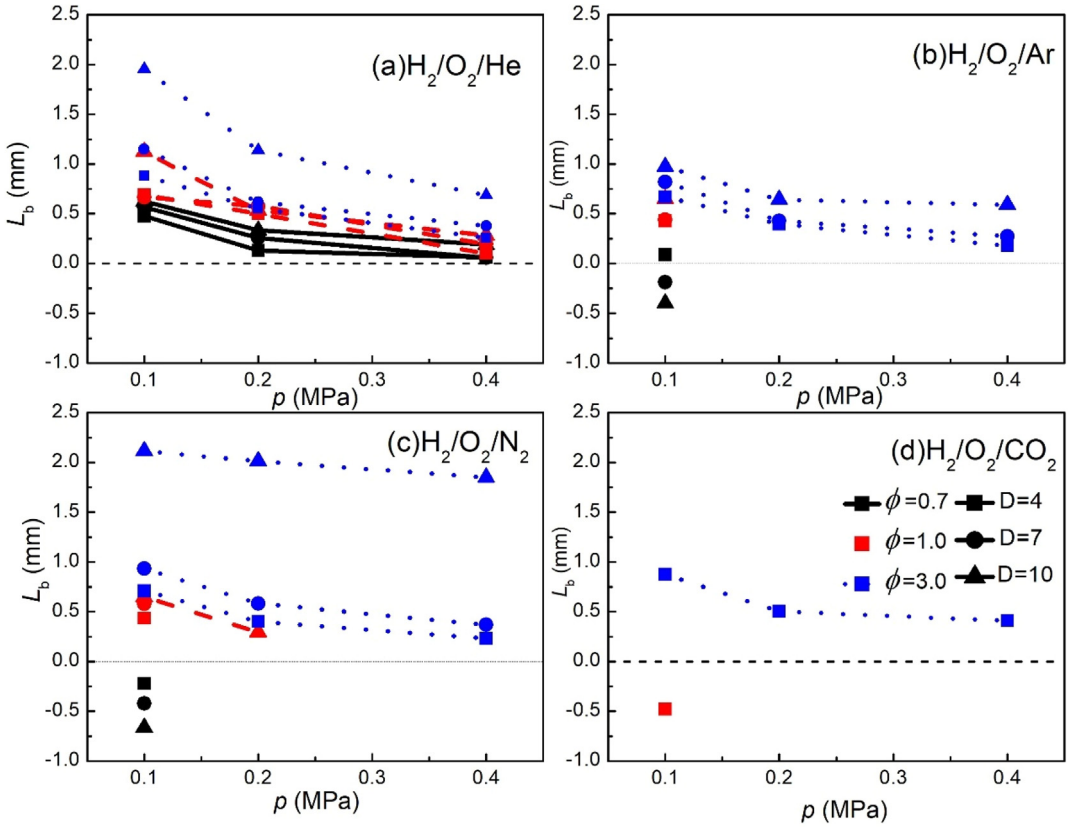

Fig. 7 – Markstein lengths of different mixtures at different conditions. (a) H_2/O_2/He, (b) H_2/O_2/Ar, (c) $H_2/O_2/N_2$, (d) $H_2/O_2/CO_2$.

multicomponent transport were considered in the calculations. The solution gradient and curvature were both set to 0.01, and the final grid number was larger than 900 to assure accuracy. The density ratio and adiabatic flame temperature were calculated using the equilibrium solver in Chemkin II [41]. The density, heat capability, and thermal conductivity of the unburned gas were calculated using Gaseq program [43].

Experimental results

Flame morphology

Fig. 3(a) shows flame images of mixtures of different diluent and equivalence ratios at $p = 0.2$ MPa with $D = 4$. It can be seen that the flame surface under the fuel-rich condition is smoother than that under the fuel-lean condition, which is mainly caused by the increase of *Le* with equivalence ratio. Under lean conditions, only a few wrinkles appeared on the flame surface of the He diluted mixture, whilst cellular structures appeared on in Ar, N_2, and CO_2 diluted mixtures. The CO_2 diluted mixture has the most wrinkled surface. At a stoichiometric equivalence ratio, fewer cracks still appear on the flame surface of the He diluted mixture. For Ar and N_2 diluted mixtures, winkles appeared on the flame surface instead of the cellular structure. The cellular structure only appeared on the flame surface of CO_2 diluted mixtures. Under fuel-rich conditions, the surface of He and CO_2 diluted flame is completely smooth, while only a few wrinkles for the Ar and N_2 diluted mixtures. It is interesting to notice that the CO_2 diluted flame is the most unstable under fuel-lean conditions, but more stable than the Ar and N_2 diluted flames under fuel-rich conditions. Further discussion of this phenomenon is presented below.

Fig. 3(b) shows the Ar diluted mixture at $\varphi = 0.7$ for different dilution ratios and different initial pressures. At the same initial pressure, the flame surface is smoother for larger dilution ratios. For a given dilution ratio, the flame surface is smoothest at 0.1 MPa. The cellular structure appears when the initial pressure increased. Also, notice that the cellular structure of the 0.4 MPa cases is denser than that of the 0.2 MPa cases. This indicated that the flame surface is more unstable at lower dilution ratios and under higher initial pressure. Further discussion of flame instability is given below.

The critical flame radius

To discuss the flame instability, the critical flame radii of different mixtures were measured. The results are shown in Fig. 4. He diluted mixtures show no cellular structure at any of the conditions considered; thus, only critical flame radii of Ar,

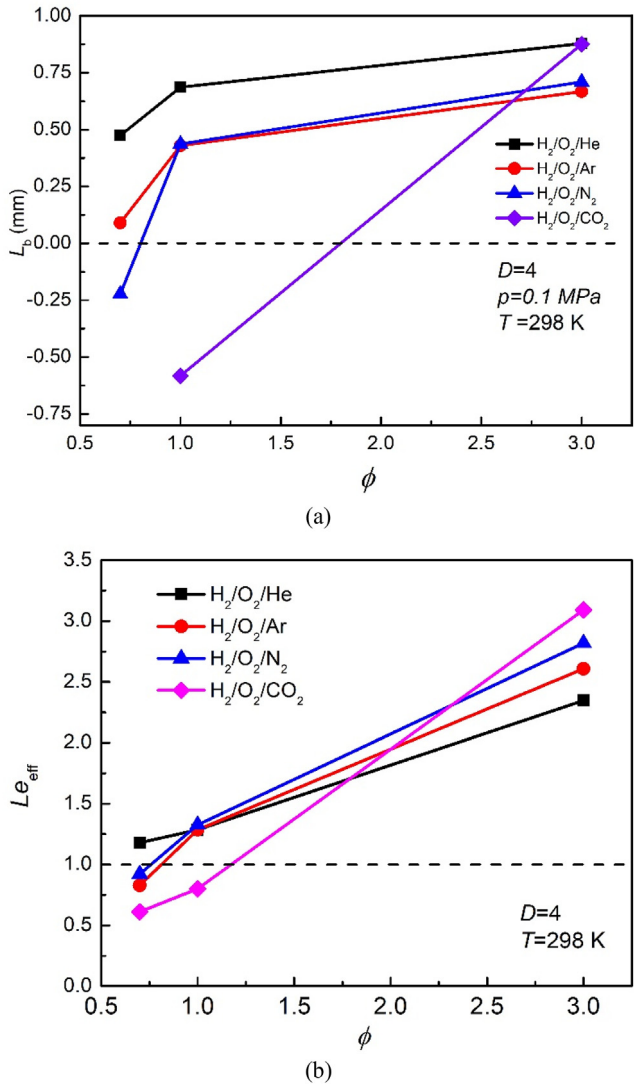

Fig. 8 – (a) Markstein lengths and (b) effective Lewis numbers of mixtures with different diluents.

N_2, and CO_2 diluted mixtures are shown. Symbols represent experiments and lines represent calculated results. The calculated results match the trends of experiments well, but the simulation results are 4–6 times smaller than experiments. The source of the difference in the magnitude is not known but is similar to that shown by previous studies (e.g. [36,44]). It can be seen that R_{cr} decreases with increasing pressure and increases with increasing dilution ratio. R_{cr} at $\phi = 0.7$ is smaller than that at $\phi = 1.0$. It can also be found that R_{cr}s of different mixtures are close to each other at $p = 0.4$ MPa. In Fig. 5, both experimental and calculated results show that R_{cr}s of all mixtures increased with the dilution ratio. Theoretical R_{cr} of He diluted mixture is calculated and it is larger than that of mixtures with other diluents. It can be seen that experimental R_{cr}s of all mixtures decrease with pressure. At a given pressure and $D = 4$, the N_2 diluted mixture has the largest experimental R_{cr} and the CO_2 diluted mixture has the smallest. Also, it can be seen that R_{cr} of the N_2 diluted mixture at$\phi = 0.7$ is smaller than that at$\phi = 1.0$.

To better understand the effects of dilution ratio, equivalence ratio, and pressure on Rcr, Pe_{cr}, flame thickness, and Le_{eff} were calculated and are shown in Fig. 6. The Le_{eff} is hardly affected by pressure according to its definition, thus only effects of diluents and dilution ratios on Le_{eff} are shown and discussed. The physical factors show influence on Rcr through their effects on Pecr and l_0, and the Pecr is affected mainly through the change of Le_{eff}. Comparing Fig. 6(a) and 6(c), it can be found that Le_{eff} dominates the tendency of Pe_{cr}. In Fig. 6(c), Le_{eff} of Ar, CO_2 and N_2 diluted mixtures decreases with increasing dilution ratio, while Le_{eff} of the He diluted mixture increases. The change of Le_{eff} leads to the change of Pe_{cr}. In Fig. 6(a), the experimentally derived Pe_{cr} of the Ar diluted mixture is larger than that of N_2 and CO_2 diluted mixtures, while the CO_2 diluted mixture has the smallest value. The He diluted mixture has the largest calculated Pe_{cr}. Calculated results of N_2 and Ar are similar and CO_2 has the smallest Pe_{cr}. Le_{eff} has a similar tendency in Fig. 6(c). The calculated results match the tendency of Pe_{cr} well, except for failing to predict that Pe_{cr} of Ar is larger than that of N_2. In Fig. 6(a), it can be seen that when the dilution ratio increases, both experimental and theoretical Pe_{cr}s decrease except for the He diluted mixture. The flame thickness increases with increasing dilution ratio Fig. 6(b). Although Pe_{cr} of N_2, CO_2, and Ar diluted mixture decreases, the increasing flame thickness with dilution ratio leads to larger R_{cr}, as shown in Fig. 5. When pressure increases, Pe_{cr} hardly changes because Le_{eff} is minimally affected by pressure. However, the flame thickness of the N_2 diluted mixture decreases with pressure, leading to decreasing R_c. Comparing the N_2 diluted mixture of different equivalence ratios, it can be found that the mixture with $\phi = 0.7$ has a smaller Le_{eff} than that at$\phi = 1.0$, thus Pe_{cr} of the$\phi = 0.7$ mixture is smaller than that of the$\phi = 1.0$ mixture. However, R_{cr} of the $\phi = 0.7$ mixture is larger than that of the $\phi = 1.0$ mixture because the $\phi = 0.7$ mixture has larger flame thickness.

The Markstein length

The Markstein length represents the sensitivity of flame speed to flame stretch and controls the preferential-diffusional stability of the flame fronts. L_bs of all the mixtures at different conditions are given in Fig. 7. Different types of symbols represent different dilution ratios and different colors represent different equivalence ratios. L_bs at some conditions are not available because of the cellular structure. It can be seen that L_bs of all mixtures decreases with increasing pressure, which suggests that the flame is less sensitive to flame stretch effects under higher pressure. At a given pressure, L_bs under fuel-rich conditions is larger than those under fuel-lean conditions. It can be found that if the value of L_b at $D = 4$ is larger than zero, then L_b will increase with the dilution ratio. If L_b has a negative value at $D = 4$, it will decrease with the dilution ratio. A similar phenomenon can also be observed in Zhang's [19] and Tatouh's [45] work.

A comparison of L_bs and Le_{eff} of mixtures with different diluents is shown in Fig. 8. In Fig. 8(b), Le_{eff} of all mixtures

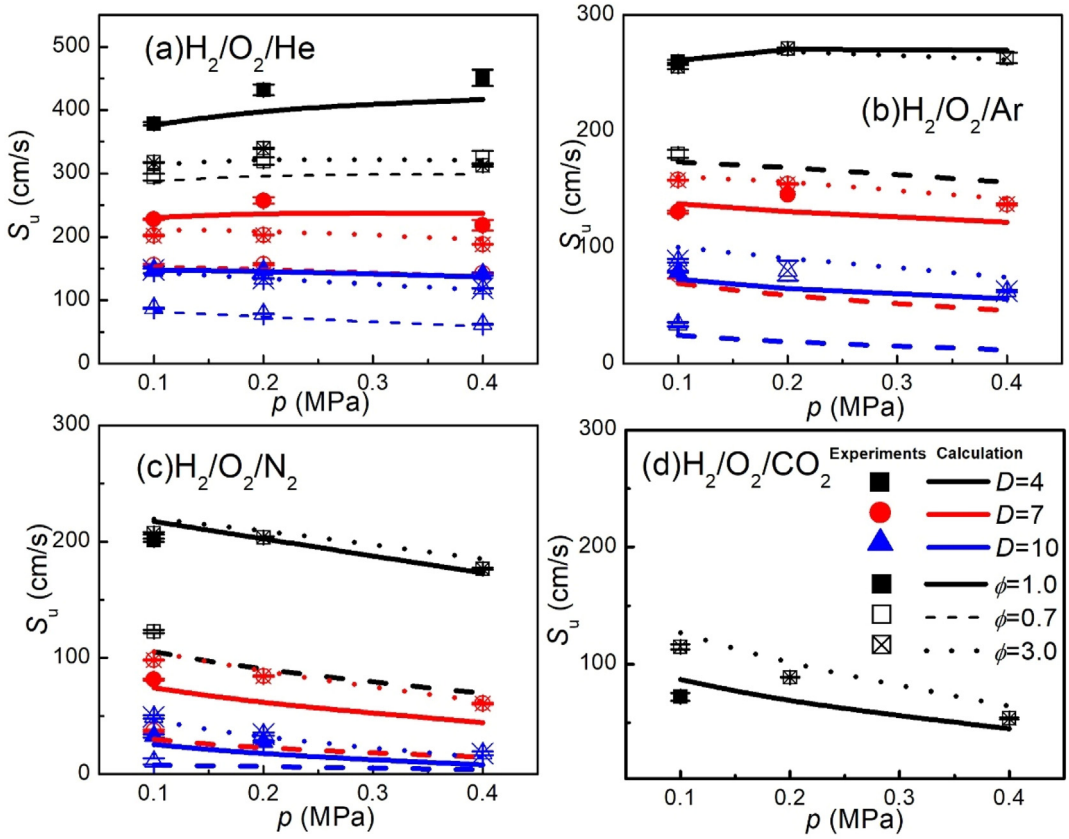

Fig. 9 – Experimental and Calculated laminar burning velocity of (a) He, (b) Ar, (c) N_2 and (d) CO_2 diluted mixtures at different conditions.

increases with equivalence ratio, which indicates that mixtures tend to be thermal diffusive stable. Thus, L_bs of all mixture also increases with the equivalence ratio in Fig. 8(a). He diluted mixtures have the largest L_b. The Le_{eff} of He diluted mixture is always larger than unity, thus L_b of He diluted mixture is always positive. L_b of the N_2 diluted mixture is smaller than that of the Ar diluted mixture under fuel-lean conditions, while L_bs of N_2 and Ar diluted mixtures are similar under stoichiometric and fuel-rich conditions. L_bs of CO_2 diluted mixtures increases rapidly with equivalence ratio. CO_2 diluted mixtures show strong instability at $\phi = 0.7$; thus, L_b is not measured. L_b of CO_2 diluted mixtures is significantly smaller than other mixtures at $\phi = 1.0$. However, L_b of CO_2 diluted mixtures is larger than that of N_2 and CO_2 diluted mixtures and similar to that of the He diluted mixture. This also validated the phenomenon observed in Fig. 3, where the CO_2 diluted mixture has the most wrinkled flame front at $\phi = 0.7$ and 1.0, but has a smooth flame surface at $\phi = 3.0$. In Fig. 8(b), it can be seen that the Le_{eff} of CO_2 increases rapidly with equivalence ratio, which can contribute to the rapid increase of L_b.

Laminar burning velocity

The laminar burning velocity of different mixtures under all experimental conditions is shown in Fig. 9. The symbols represent the experiments and the lines represent the calculated results. Mixtures with different dilution ratios are represented using different colors and mixtures of different equivalence ratios are shown using different types of scatters and lines. The calculations match the experiments well under most conditions.

Fig. 10(a) shows the S_u of different diluted mixtures under different initial pressures. The He diluted mixture had the largest Su and the Ar diluted mixture was the second. The N_2 diluted mixture has slower Su than He and Ar diluted mixtures and the CO_2 diluted mixture has the slowest S_u. The reason for CO_2 having the slowest S_u is that CO_2 has a larger heat capacity than other diluents, and T_{ad} of the CO_2 diluted mixture is lower than others, which decreases S_u. The reason of He and Ar diluted mixtures had faster S_u than N_2 diluted mixtures is also because of the smaller heat capacity of He and Ar, which could lead to higher T_{ad}. The He diluted mixture has a faster S_u than the Ar diluted mixture because the He diluted mixture has stronger diffusivity. The calculated results accurately match the Ar and N_2 diluted mixtures, and the calculations are slightly lower than S_u of He diluted mixture, while a little higher than that of CO_2 diluted mixture. When pressure increases, S_u of the He and Ar diluted mixtures slightly increases as first and then decreases, while S_u of N_2 and CO_2 diluted mixtures monotonically decreases with increasing pressure. Fig. 10(b) shows S_u of He diluted mixture of different dilution ratios and different pressures. The calculated results match the experiments well. Burke's model accurately predicted Sus at D = 7 and 10, while slightly underestimate at $D = 4$. It can be found that both measured and calculated

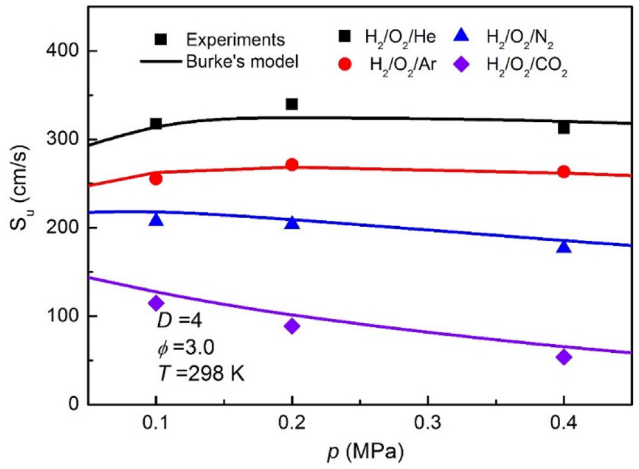

(a)

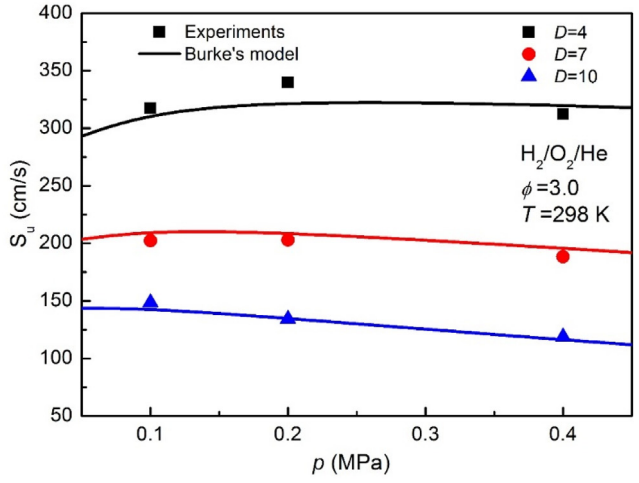

(b)

Fig. 10 – Laminar burning velocities of (a) mixtures with different diluents as a function of pressure and (b) Helium diluted mixture at $\phi = 3.0$ and under different dilution ratios and pressures.

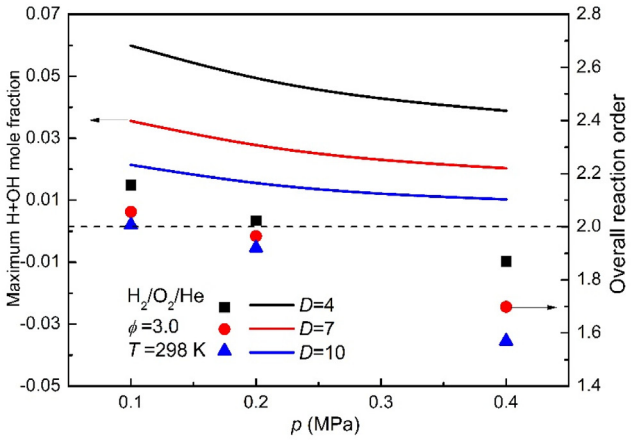

(a)

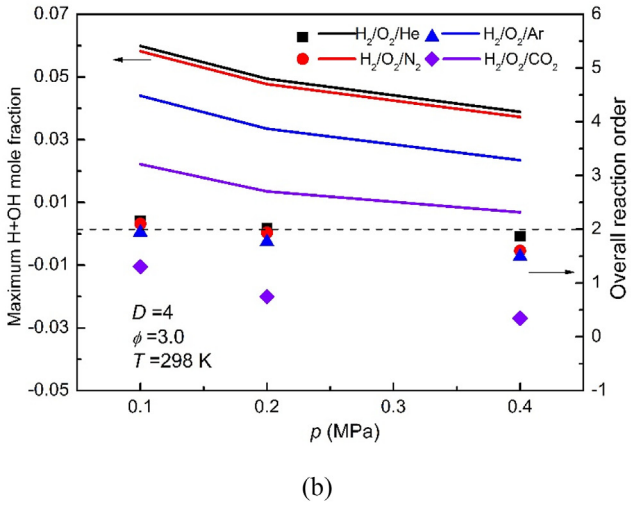

(b)

Fig. 11 – Overall reaction order and H+OH radicals as a function of (a) p = 0.2 MPa and (b) D = 4.

laminar velocities of $D = 4$ increase at first, then decrease with increasing pressure. At $D = 7$, both experiments and calculations show similar tendencies to that of D = 4, while the increase of S_u is slower than that of $D = 4$. However, at $D = 10$, the results show that S_u only decreases with increasing pressure monotonically. It can be seen that there is a non-monotonic behavior of S_u as a function of initial pressure, and the increase of the dilution ratio can restrain this behavior.

The overall reaction rate, ω, determines the mass burning rate and it is given by [35].

$$\omega \sim p^{n}\exp(-Ea/2RT_{ad}), \tag{13}$$

where n is the overall reaction order. It can be seen that ω has an exponential relationship with pressure, and this exponential value is defined as the overall reaction order, which indicates the intensity of overall reactions. The relationship between S_u and pressure can be expressed as

$$S_u \sim p^{\frac{n}{2}-1}\exp\left(-\frac{Ea}{2RT_{ad}}\right). \tag{14}$$

It can be noticed that S_u will increase with pressure if n > 2 and decreases with pressure if n < 2. The relationship between f_0 and pressure can also be expressed as

$$f_0 \sim p^{\frac{n}{2}}\exp(-Ea/2R^0T_{ad}). \tag{15}$$

Thus, the overall reaction order can be obtained by

$$n = 2\partial\ln(f_0)/\partial\ln(p). \tag{16}$$

To better show the nonmonotonic behavior of S_u with increasing pressure, the overall reaction order, n, is calculated and shown in Fig. 11. The maximum H+OH radical mole fraction indicates the activated radical concentration, which contributes to the overall reactions. To discuss the effects of

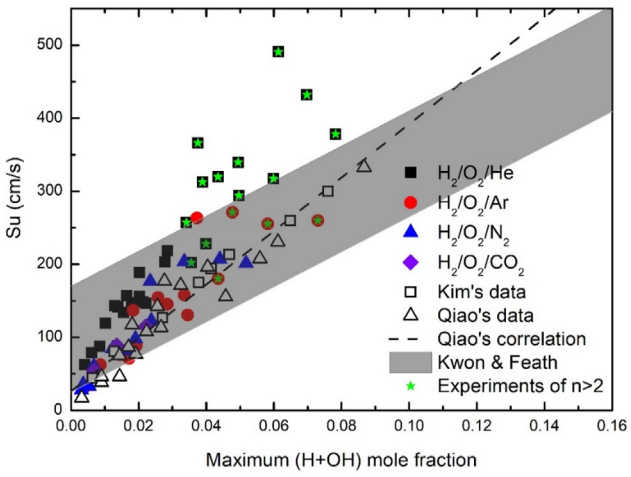

(a)

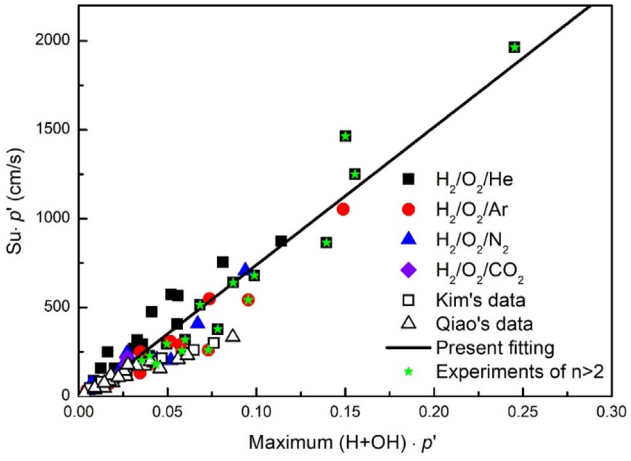

(b)

Fig. 12 – Relation between Su and H+OH radical with (a) original empirical equation and (b) present the modified empirical equation.

radical concentration, the maximum H+OH mole fraction is also plotted in Fig. 11.

In Fig. 11(a), it can be seen that both the maximum H+OH mole fraction and overall reaction order decreased when dilution ratio and pressure increase. When the dilution ratio increases, the radical concentration is reduced and the overall reaction order decreases. When pressure increases, the main chain-branching reactions, $H+O_2 = O+OH$ and $O+H_2 = H+OH$, are restrained. However, the three-body reaction, $H+O_2(+M) = HO_2(+M)$, is promoted and consumes more H radicals. Thus, the activated radical concentration is reduced and the max H+OH mole fraction decreases with pressure. The reduction of the radical pool can lead to a decrease in reaction intensity and the overall reaction order. Overall reaction orders of D = 4 and 7 are larger than 2 at low pressure and smaller than 2 at high pressure. Thus, the S_u of these two mixtures increases with pressure initially and decreases afterward. For mixture D = 10, the overall reaction order is almost 2 at 0.1 MPa and less than 2 at higher pressures, indicating that the S_u of D = 10 should decrease with pressure monotonically. The change of S_u matches the results in Fig. 10.

In Fig. 11(b), both maximum H+OH and the overall reaction order decrease with initial pressure. The maximum H+OH and overall reaction order of the He diluted mixture are the largest, then follows those of Ar and N_2 diluted mixtures, and the CO_2 diluted mixture has the lowest values, consisted of the order of laminar burning velocity. It can be seen that overall reaction orders of He and Ar diluted mixtures are larger than 2 at low pressure, and the values reduce to less than 2 at high pressure. This leads to the nonmonotonic behavior in Fig. 10. The chemical reason for the decrease of overall reaction order is that the increasing pressure leads to a smaller radical pool, and further leads to the decrease of overall reaction order, as discussed above.

Kim [24], Kwon [25] and Qiao [12] reported that the H and OH radical has a strong correlation between Su and the maximum concentration of H and OH radicals. In Fig. 12, it can be seen that the old correlations fail to predict the experiments that show nonmonotonic behavior with pressure. Because the pressure of past work is limited to atmospheric pressure, the original correlations are not likely to capture the pressure effects. In Fig. 12(a), it can be seen that experiments of n > 2 exceeds the prediction region of past studies. Because of the nonmonotonic behavior, S_u increases with decreasing maximum H+OH when pressure increases. Thus, previous correlations failed to capture these data. With the pressure effects considered, a new linear correlation is proposed as

$$S_u \cdot p' = -40 + 7760 \cdot Max(H+OH) \cdot p', \quad (17)$$

where $Max(H+OH)$ represents the maximum value of mole fraction of H and OH radicals, $p' = p/p_0$ is the pressure coefficient and p_0 is 0.1 MPa in this study. The left side of Eq. (17) represents the mass flow rate and the right side represents the concentration of radicals. The new correlation line is compared with current and previous experiments, as shown in Fig. 12(b). It can be seen that the new correlation matches experiments well and is slightly higher than Qiao's and Kim's data. Likewise, the data of n > 2 is still in the range of the current data region.

Conclusion

Laminar flame characteristics of a hydrogen flame with four different diluents, He, Ar, N_2, CO_2, were studied with different diluent concentrations and different equivalence ratios. Critical flame radii were measured to study flame instability. Theoretical results were also calculated to analyze the effects of different physical factors. The results show that R_{cr} decreases with pressure and increases with equivalence ratio and dilution ratio, which indicates that flame instability is enhanced at higher pressure, smaller equivalence ratio, and dilution ratio. He diluted mixture has no experimental R_{cr} because the flame is always smooth. N_2 diluted mixture has the largest experimental R_{cr}, while the CO_2 diluted mixture has the smallest. R_{cr} is influenced by both critical Peclet number and

flame thickness. The calculations reveal that critical Peclet numbers of Ar, N_2, and CO_2 diluted mixtures decrease with dilution ratio, which is caused by the decrease of Le_{eff}. However, the flame thickness of the mixture increases and results in an increasing R_{cr}. The Peclet number of He diluted mixtures slightly increases because Le_{eff} of He diluted mixture increases.

Markstein lengths were measured to show the sensitivity to flame stretch. The results show that L_b decreases with pressure and increases with equivalence ratio. It is interesting to found that L_b of CO_2 diluted mixture increase rapidly from the lowest at $\phi = 1.0$ to a high value at $\phi = 3.0$, which indicates the CO_2 diluted flame has the most cellular-structured flame surface under fuel-lean conditions and a rather smooth flame front under fuel-rich conditions. The flame images show the same behavior that the CO_2 diluted mixture has most unstable flame front at $\phi = 0.7$, 1.0, and tends to be smoother than other mixtures at $\phi = 3.0$. The reason is that Le_{eff} of CO_2 diluted mixture increases rapidly from the smallest value at$\phi = 0.7$ to the highest value at $\phi = 3.0$, which indicates that the thermal diffusion instability of CO_2 increases with equivalence ratio faster than that of other mixtures.

Laminar burning velocities of all mixtures were measured. At a given experimental condition, He diluted mixtures have the fastest S_u and the CO_2 diluted mixtures have the slowest S_u. The reason is that different diluents have different C_p, which has a significant influence on flame temperature and S_u. For example, CO_2 has large heat capacity due to the three-atom structure, which leads to a low adiabatic flame temperature then results in a slow S_u. The results show that S_u decreases with dilution ratio because the radical concentration is reduced due to increasing diluent concentration. It can be found that S_u with Ar and He diluents shows non-monotonic behavior at low dilution ratios. The calculated results indicated that this is caused by the reduction of the reaction order from above 2 to below 2, which is caused by the reduction of radical pool with increasing pressure. It can also be found the past empirical relation between S_u and activated radicals fails to predict current non-monotonic experimental data. A modified equation was presented and found to match the present and previous experiments well.

Declaration of competing interest

The authors declare that they have no known competing financial interests or personal relationships that could have appeared to influence the work reported in this paper.

Acknowledgments

This work is supported by the Basic Science Center Program for Ordered Energy Conversion of the National Natural Science Foundation of China (51888103), the Natural Science Foundation of Shaanxi Province for Distinguished Young Scholars (2020JC-04), the scholarship from the Chinese Scholar Council (201906280337) and Young Talent Support Plan of Shaanxi Province. The supports from Science and Technology on Combustion, Internal Flow and Thermal-structure Laboratory (6142701190401), and the Fundamental Research Funds for the Central Universities and are also appreciated.

REFERENCES

[1] Liu X-h, Liu F-s, Zhou L, Sun B-g, Schock HJ. Backfire prediction in a manifold injection hydrogen internal combustion engine. Int J Hydrogen Energy 2008;33:3847–55.
[2] Eichlseder H, Wallner T, Freymann R, Ringler J. The potential of hydrogen internal combustion engines in a future mobility scenario. SAE Technical Paper. 2003.
[3] Yamada N, Mohamad MNA. Efficiency of hydrogen internal combustion engine combined with open steam Rankine cycle recovering water and waste heat. Int J Hydrogen Energy 2010;35:1430–42.
[4] Mori D, Hirose K. Recent challenges of hydrogen storage technologies for fuel cell vehicles. Int J Hydrogen Energy 2009;34:4569–74.
[5] Jacobson MZ, Colella W, Golden DM. Cleaning the air and improving health with hydrogen fuel-cell vehicles. Science 2005;308:1901–5.
[6] Frenette G, Forthoffer D. Economic & commercial viability of hydrogen fuel cell vehicles from an automotive manufacturer perspective. Int J Hydrogen Energy 2009;34:3578–88.
[7] Westbrook CK, Dryer FL. Chemical kinetic modeling of hydrocarbon combustion. Prog Energy Combust Sci 1984;10:1–57.
[8] Aung KT, Hassan MI, Faeth GM. Flame stretch interactions of laminar premixed hydrogen/air flames at normal temperature and pressure. Combust Flame 1997;109:1–24.
[9] Cai X, Wang J, Bian Z, Zhao H, Dai H, Huang ZH, et al. On transition to self-similar acceleration of spherically expanding flames with cellular instabilities. Combust Flame 2020;215:364–75.
[10] Wu F, Jomaas G, Law CK. An experimental investigation on self-acceleration of cellular spherical flames. Proc Combust Inst 2013;34:937–45.
[11] Kim WK, Mogi T, Kuwana K, Dobashi R. Self-similar propagation of expanding spherical flames in large scale gas explosions. Proc Combust Inst 2015;35:2051–8.
[12] Qiao L, Kim C, Faeth G. Suppression effects of diluents on laminar premixed hydrogen/oxygen/nitrogen flames. Combust Flame 2005;143:79–96.
[13] Qiao L, Gu Y, Dahm WJA, Oran ES, Faeth GM. A study of the effects of diluents on near-limit H_2–air flames in microgravity at normal and reduced pressures. Combust Flame 2007;151:196–208.
[14] Paidi SK, Bhavaraju A, Akram M, Kumar S. Effect of N_2/CO_2 dilution on laminar burning velocity of H_2–air mixtures at high temperatures. Int J Hydrogen Energy 2013;38:13812–21.
[15] Hu E, Huang Z, He J, Jin C, Miao H, Wang X. Measurement of laminar burning velocities and analysis of flame stabilities for hydrogen-air-diluent premixed mixtures. Sci Bull 2009;54:846–57.
[16] Shang R, Zhang Y, Zhu M, Zhang Z, Zhang DJE, Fuels. Semiempirical correlation for predicting laminar flame speed of H_2/CO/air flames with CO_2 and N_2 dilution. Energy Fuels 2017;31:9957–66.
[17] Lee MC, Seo SB, Yoon J, Kim M, Yoon YJF. Experimental study on the effect of N2, CO2, and steam dilution on the combustion performance of H2 and CO synthetic gas in an industrial gas turbine. Fuel 2012;102:431–8.
[18] Miao H, Ji M, Jiao Q, Huang Q, Huang Z. Laminar burning velocity and Markstein length of nitrogen diluted natural

gas/hydrogen/air mixtures at normal, reduced and elevated pressures. Int J Hydrogen Energy 2009;34:3145–55.
[19] Zhang X, Huang Z, Zhang Z, Zheng J, Yu W, Jiang D. Measurements of laminar burning velocities and flame stability analysis for dissociated methanol–air–diluent mixtures at elevated temperatures and pressures. Int J Hydrogen Energy 2009;34:4862–75.
[20] Lu X, Hu E, Li X, Ku J, Huang Z. Non-monotonic behaviors of laminar burning velocities of H_2/O_2/He mixtures at elevated pressures and temperatures. Int J Hydrogen Energy 2017;42:22036–45.
[21] Tse SD, Zhu DL, Law CK. Morphology and burning rates of expanding spherical flames in H_2/O_2/inert mixtures up to 60 atmospheres. Proc Combust Inst 2000;28:1793–800.
[22] Yang S, Yang X, Wu F, Ju Y, Law CK. Laminar flame speeds and kinetic modeling of H2/O2/diluent mixtures at sub-atmospheric and elevated pressures. Proc Combust Inst 2017;36:491–8.
[23] Kwon S, Tseng LK, Faeth GM. Laminar burning velocities and transition to unstable flames in $H_2/O_2/N_2$ and $C_3H_8/O_2/N_2$ mixtures. Combust Flame 1992;90:230–46.
[24] Kim C, Kwon O, Faeth G. Effects of halons and halon replacements on hydrogen-fueled laminar premixed flames. J Propul Power 2002;18:1059–67.
[25] Kwon O, Faeth GC. Flame/stretch interactions of premixed hydrogen-fueled flames: measurements and predictions. Combust Flame 2001;124:590–610.
[26] Hu E, Huang Z, He J, Jin C, Zheng J. Experimental and numerical study on laminar burning characteristics of premixed methane–hydrogen–air flames. Int J Hydrogen Energy 2009;34:4876–88.
[27] Tang C, Huang Z, Jin C, He J, Wang J, Wang X, et al. Laminar burning velocities and combustion characteristics of propane–hydrogen–air premixed flames. Int J Hydrogen Energy 2008;33:4906–14.
[28] Xiouris C, Ye T, Jayachandran J, Egolfopoulos FN. Laminar flame speeds under engine-relevant conditions: uncertainty quantification and minimization in spherically expanding flame experiments. Combust Flame 2016;163:270–83.
[29] Xie Y, Wang J, Cai X, Huang Z. Self-acceleration of cellular flames and laminar flame speed of syngas/air mixtures at elevated pressures. Int J Hydrogen Energy 2016;41:18250–8.
[30] Bauwens CR, Bergthorson JM, Dorofeev SB. Experimental study of spherical-flame acceleration mechanisms in large-scale propane–air flames. Proc Combust Inst 2015;35:2059–66.
[31] Katsumi T, Aida T, Aiba K, Kadowaki S. Outward propagation velocity and acceleration characteristics in hydrogen-air deflagration. Int J Hydrogen Energy 2017;42:7360–5.
[32] Burke MP, Chen Z, Ju Y, Dryer FL. Effect of cylindrical confinement on the determination of laminar flame speeds using outwardly propagating flames. Combust Flame 2009;156:771–9.
[33] Savitzky A, Golay MJE. Smoothing and differentiation of data by simplified least squares procedures. Anal Chem 1964;36:1627–39.
[34] Addabbo R, Bechtold JK, Matalon M. Wrinkling of spherically expanding flames. Proc Combust Inst 2002;29:1527–35.
[35] Egolfopoulos FN, Law CK. Chain mechanisms in the overall reaction orders in laminar flame propagation. Combust Flame 1990;80:7–16.
[36] Bechtold JK, Matalon M. The dependence of the Markstein length on stoichiometry. Combust Flame 2001;127:1906–13.
[37] Moffat RJ. Describing the uncertainties in experimental results. Exp Therm Fluid Sci 1988;1:3–17.
[38] Yu H, Han W, Santner J, Gou X, Sohn CH, Ju Y, et al. Radiation-induced uncertainty in laminar flame speed measured from propagating spherical flames. Combust Flame 2014;161:2815–24.
[39] Lu X, Hu E, Xu Z, Ge R, Huang Z, Zeng KJF. Non-monotonic behavior of flame instability of 1, 3-butadiene/O2/He mixture up to 1.5 MPa. Fuel 2019;255:115749.
[40] Burke MP, Chaos M, Ju Y, Dryer FL, Klippenstein SJ. Comprehensive H2/O2 kinetic model for high-pressure combustion. Int J Chem Kinet 2011;44:444–74.
[41] Rupley FM, Kee RJ, Miller JA. CHEMKIN-2: a FORTRAN chemical kinetics package for the analysis of gas-phase chemical kinetics. 1989.
[42] Kee RJ, Grcar JF, Smooke MD, Miller JA, Meeks E. PREMIX. A Fortran program for modeling steady laminar one-dimensional premixed flames, 143; 1985. p. 65.
[43] Morley C. Gaseq,Version 0.76. http://wwwgaseqcouk/. 2005.
[44] Okafor EC, Nagano Y, Kitagawa T. Experimental and theoretical analysis of cellular instability in lean H_2 -CH_4 -air flames at elevated pressures. Int J Hydrogen Energy 2016;41:6581–92.
[45] Tahtouh T, Halter F, Samson E, Mounaïm-Rousselle C. Effects of hydrogen addition and nitrogen dilution on the laminar flame characteristics of premixed methane–air flames. Int J Hydrogen Energy 2009;34:8329–38.